



Quinolinetrione-tacrine hybrids as multi-target-directed ligands against Alzheimer's disease[☆]

Elisa Uliassi^a, Christian Bergamini^a, Nicola Rizzardi^a, Marina Naldi^a, Ángel Cores^b,
Manuela Bartolini^a, J. Carlos Menéndez^{b,*}, Maria Laura Bolognesi^{a,*}

^a Department of Pharmacy and Biotechnology, Alma Mater Studiorum – University of Bologna, 40126 Bologna, Italy

^b Department of Chemistry in Pharmaceutical Sciences, Organic and Medicinal Chemistry Unit, Faculty of Pharmacy, Universidad Complutense, 28040 Madrid, Spain

ARTICLE INFO

Keywords:

Polypharmacology
Multi-target-directed ligands
Alzheimer's disease
Cholinesterase enzymes
Amyloid- β
Tacrine
Quinolinetrione

ABSTRACT

Multi-target drug discovery is one of the most active fields in the search for new drugs against Alzheimer's disease (AD). This is because the complexity of AD pathological network might be adequately tackled by multi-target-directed ligands (MTDLs) aimed at modulating simultaneously multiple targets of such a network. In a continuation of our efforts to develop MTDLs for AD, we have been focusing on the molecular hybridization of the acetylcholinesterase inhibitor tacrine with the aim of expanding its anti-AD profile. Herein, we manipulated the structure of a previously developed tacrine-quinone hybrid (**1**). We designed and synthesized a novel set of MTDLs (**2–6**) by replacing the naphthoquinone scaffold of **1** with that of 2,5,8-quinolinetrione. The most interesting hybrid **3** inhibited cholinesterase enzymes at nanomolar concentrations. In addition, **3** exerted antioxidant effects in menadione-induced oxidative stress of SH-SY5Y cells. Importantly, **3** also showed low hepatotoxicity and good anti-amyloid aggregation properties. Remarkably, we uncovered the potential of the quinolinetrione scaffold, as a novel anti-amyloid aggregation and antioxidant motif to be used in further anti-AD MTDL drug discovery endeavors.

1. Introduction

Alzheimer's disease (AD) is a neurodegenerative condition and the main form of dementia, characterized by a cognitive impairment compromising independence and affecting daily life.¹ Today, 55 million people live with a diagnosis of dementia. That number is expected to grow to 139 million in 2050.²

Drug discovery in AD has been punctuated by setbacks and high promises. Cholinesterase inhibitors (ChEIs) developed three decades ago, together with memantine (2003), an antagonist to *N*-methyl-D-aspartate receptor, are still the first choice in AD treatment. Although cholinergic deficit was recognized as the first AD pathological alteration associated with memory deficits and cognitive decline, ChEIs offer a merely symptomatic relief. ChEIs, such as rivastigmine, donepezil, and

galantamine, restore cholinergic transmission mainly by preventing the hydrolysis of acetylcholine by acetylcholinesterase (AChE), thus slowing the decline of cognitive functions. Non selective activity and inhibition of the hydrolytic activity of the non-specific cholinesterase enzyme butyrylcholinesterase (BChE) is thought to also contribute to their action. Indeed, novel relationships between AChE/BChE and other pathological features of AD are being discovered.^{3,4}

While AD etiology is still poorly understood, the presence of β -amyloid (A β) plaques in nearly 80% of AD cases had suggested A β as a leading AD driver.⁵ Although several A β -centric programs failed over decades, making the scientific community skeptical about the validity of the so-called amyloid hypothesis, the clinical approval of aducanumab in 2021 and lecanemab in 2023 has led to a reconsideration of such hypothesis.⁶ However, the accelerated approval of these amyloid-

Abbreviations: AD, Alzheimer's disease; MTDLs, multi-target-directed ligands; ChEIs, cholinesterase inhibitors; AChE, acetylcholinesterase; BChE, butyrylcholinesterase; A β , amyloid- β ; ROS, reactive oxygen species; CAN, cerium ammonium nitrate.

[☆] We dedicate this article with gratitude to Prof. Carlo Melchiorre, who pioneered multi-target drug discovery in Alzheimer's disease, on the occasion of his 80th birthday.

* Corresponding authors at: Department of Chemistry in Pharmaceutical Sciences, Organic and Medicinal Chemistry Unit, Faculty of Pharmacy, Universidad Complutense, 28040 Madrid, Spain (J. Carlos Menéndez). Department of Pharmacy and Biotechnology, Alma Mater Studiorum—University of Bologna, Via Belmeloro 6, I-40126 Bologna, Italy (M.L. Bolognesi).

E-mail addresses: josecm@farm.ucm.es (J. Carlos Menéndez), marialaura.bolognesi@unibo.it (M.L. Bolognesi).

<https://doi.org/10.1016/j.bmc.2023.117419>

Received 12 May 2023; Received in revised form 4 July 2023; Accepted 18 July 2023

Available online 19 July 2023

0968-0896/© 2023 The Authors. Published by Elsevier Ltd. This is an open access article under the CC BY license (<http://creativecommons.org/licenses/by/4.0/>).

removing antibodies is still matter of controversy, as they appear to show limited benefits by moderately slowing cognitive decline only at early-disease stages and even potential toxicity.⁷ Nevertheless, interest in anti-amyloid small molecules, being cheaper to produce and easier to administer than antibodies, continues to be on the rise.⁸

Oxidative damage, i.e., the imbalance in radical production of reactive oxygen species (ROS) and antioxidative defense, is another key component of AD pathology.^{9,10,11,12} An increased oxidation of brain lipids, carbohydrates, proteins, and DNA has been found in the major AD histopathologic alterations.¹² In 2022, three agents counteracting oxidative stress (hydralazine, icosapent ethyl, omega-3) represented 14.3% of the total disease-modifying treatments in phase 3.¹³ However, all clinical studies conducted so far demonstrated no clear beneficial effects in AD patients.¹⁴

Based on the multifactorial and complex nature of AD, poly-pharmacology is a therapeutic option that has led to clinical translation. Namzaric®, a combination of donepezil and memantine, was approved by FDA in 2014,¹⁵ although EMA has refused marketing authorization. Last year, a trial for evaluating the efficacy of lecanemab combined with a tau-reducing antibody was launched.¹⁶ However, combination therapies are complex and expensive to manage, especially in the case of antibodies, which need to be intravenously administered by specialized staff.¹⁶ By contrast, the polypharmacological option based on multi-target-directed ligands (MTDLs),¹⁷ i.e., single small-molecules simultaneously modulating multiple targets of the AD pathological network, seems a more promising strategy in terms of efficacy, toxicity, and costs.¹⁵ In fact, being a single small molecule-based therapy, MTDLs possess several benefits: (i) simpler pharmacokinetics that enables the simultaneous modulation of multiple targets; (ii) no metabolism-related toxicity issues arising from multiple drug intake; (iii) improved patient compliance due to simplification of the therapeutic regimen, (iv) cost-effectiveness with regard to the manufacturing compared to combination therapy.¹⁷

Our long-standing interest in the field (initiated with the publication of the perspective article by Melchiorre et al.¹⁷) prompted us to develop novel MTDLs by manipulating the structure of a previously developed quinone-tacrine hybrid **1** that exhibited a promising anti-AD profile (Fig. 1).¹⁸ **1** was rationally designed by combining tacrine, the first registered -ChEI for AD, and a naphthoquinone moiety, as an anti-

amyloid and antioxidant privileged motif.¹⁸ Indeed, **1** was able to: (1) inhibit human AChE (hAChE) in the subnanomolar range ($IC_{50} = 0.72$ nM), (2) block A β aggregation (% inhibition: 37.5% at 10 μ M) (3) exert antioxidant effects in T67 cells at 10 μ M. In addition, **1** demonstrated low neurotoxicity and a favorable blood brain barrier (BBB) permeation, but it also showed cellular hepatotoxicity when tested at 10 μ M concentration. Thus, we set out to modify the structure of **1** to improve its therapeutic profile. While keeping the tacrine moiety, because of its synthetic accessibility, ligand efficiency and suitability for the design of ChEIs and anti-AD hybrids,^{19,20} we envisioned to replace the 5-hydroxy-1,4-naphthoquinone (juglone) scaffold of **1**. This is mainly because it might be associated to toxic effects,^{21,22} although recognized as an important substructure in the development of hybrid molecules against AD.²³ Looking for a suitable replacement, we were attracted by the 2,5,8 (1H)-quinolinetrione scaffold. Indeed, the quinolinetrione should in principle retain the same beneficial features of juglone, i.e., the anti-amyloid and antioxidant properties. Being a hydrophobic and planar system, quinolinetrione might similarly perturb the A β aggregation process.¹⁸ In addition, the quinolinetrione moiety might mimic the hydrogen bond capability of the juglone fragment, thanks to the presence of the amide -NH. Both these features have been recognized as important determinants of anti-amyloid aggregation motifs.^{18,24,25} Likewise, quinolinetrione, featuring a *para*-benzoquinone core, might participate in diverse electron transfer and proton-coupled electron transfer processes, thus presumably acting as antioxidant. Furthermore, to the best of our knowledge, biological/toxicity studies on quinolinetrione derivatives are limited to a single report assessing their antitumor activity,²⁶ making the evaluation of its biological potential in AD particularly interesting.

Herein, we report the design, synthesis, and biological evaluation of a small set of quinolinetrione-tacrine hybrids **2-6** (Fig. 1).

2. Results and discussion

2.1. Design

Since cholinergic deficits, amyloid pathway, and oxidative stress are intertwined linked in AD pathological network, we were interested in manipulating the structure of **1** with the aim of improving its therapeutic

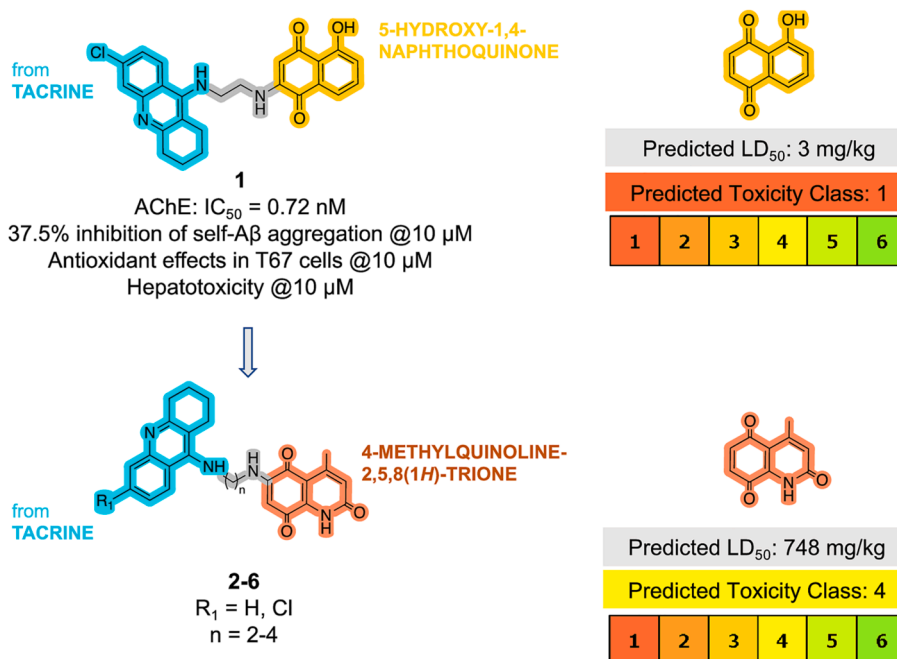


Fig. 1. Design strategy leading to quinolinetrione-tacrine hybrids **2-6**.

profile. While we maintained the tacrine fragment, essential for ChE inhibition, we sought to replace the anti-amyloid and antioxidant juglone scaffold with that of 2,5,8(1*H*)-quinolinetrione, always tethered via a methylene-based linker (Fig. 1). Previously quinone-tacrine hybrids allowed us to identify a spacer of two to four methylenes as the optimal distance allowing the proper fitting within the enzyme gorge, whilst preserving the anti-amyloid and antioxidant properties. Thus, we focused our design on the two potent tacrine derivatives (unsubstituted-tacrine and 6-chlorotacrine, which showed an improved AChE inhibitory profile with respect to the unsubstituted one)¹⁸ connected via a linker of two/four methylene units to the 4-methylquinoline-2,5,8(1*H*)-trione. An *in silico* toxicity profiling by using ProTox-II webserver,²⁷ which provides prediction of various toxicity endpoints through structure analysis and comparison to known toxicophores/toxic fragments, further supported our design (Fig. 1). 4-Methylquinoline-2,5,8(1*H*)-trione was predicted to belong to the toxicity class 4/6, in comparison to the class 1/6 of juglone, with a good degree of safety (median lethal dose, LD₅₀ = 748 mg/kg vs. LD₅₀ = 3 mg/kg). Furthermore, the toxicity radar charts and reports including prediction of acute toxicity, hepatotoxicity, and toxicological pathways (Figure S1 and Tables S1-S2) mirrored a safer profile for 4-methylquinoline-2,5,8(1*H*)-trione across all calculated categories (with the exception of carcinogenicity) with respect to 5-hydroxy-1,4-naphthoquinone. Based on these studies, we came up with a first set of quinolinetrione-tacrine hybrids 2–6, as shown in Fig. 1.

Before performing the synthesis, we also predicted the drug-likeness and the BBB permeability profile of the designed hybrids. Preliminary *in silico* drug-likeness of 2–6 in comparison with parent compound 1 was carried out using FAF-Drugs4 (Table 1).²⁸ Particularly, we considered all relevant parameters to the Lipinski's rule of five: the molecular weight (MW), the octanol–water partitioning coefficient (logP), the number of H-bond acceptors (HBA) and donors (HBD), and the number of rotatable bonds. The topological polar surface area (tPSA) and putative oral bioavailability have been also estimated. All new hybrids 2–6 were compliant to the Lipinski's rule of five, whereas 1 showed one Lipinski violation, related to a high lipophilicity (logP > 5). Nevertheless, a good oral bioavailability was predicted for all compounds. We also estimated *in silico* the ability of 2–6 to cross the BBB using the online BBB predictor (<https://www.cbiligand.org/BBB/predictor.php>) within the AlzPlatform.²⁹ Importantly, all hybrids appeared to be BBB permeable. Of note, parent compound 1 was previously demonstrated to cross the BBB in *ex vivo* experiments with rats¹⁸ and considering its structural similarity with the current series, we might assume a similar behavior for this new class of MTDLs.

2.2. Chemistry

The synthetic pathway used to obtain hybrids 2–6 followed the protocol described by Nepovimova et al.¹⁸ (Scheme 1). The synthesis of tacrines 7–8 has been previously reported.³⁰ These were exploited as key starting materials for the production of intermediates 9–13 in good to excellent yields (63–95%), by reaction with the appropriate alkylendiamines in phenol under microwave irradiation.³¹ On the other hand, the key intermediate 4-methylquinoline-2,5,8(1*H*)-trione 14 was obtained by three consecutive reactions between the commercially

available 2,5-dimethoxyaniline and 2,2,6-trimethyl-1,3-dioxin-4-one (Scheme 2).³² The first step relied on an acetoacetylation of 2,5-dimethoxyaniline with acetylketene, generated *in situ* from the dioxinone derivative via a thermal retro oxa-Diels-Alder reaction, to generate 2,5-dimethoxyacetoacetanilide 15. In the following step, treatment with sulfuric acid enabled the Knorr cyclization of 15 and its subsequent dehydration, affording the 5,8-dimethoxy-4-methyl-2(1*H*)-quinolinone 16. In the last step, 4-methylquinoline-2,5,8(1*H*)-trione 14 was obtained by oxidative demethylation of 16 with cerium ammonium nitrate (CAN) in acetonitrile (Scheme 2).

With key intermediates in hand, the reaction of alkylendiamino-1,2,3,4-tetrahydroacridines 9–13 and quinone 14 provided final compounds 2–6 in poor to moderate yields (23–45%, Scheme 1). Hybrids 2–6 have been characterized by elemental analysis, NMR spectroscopy, and ESI mass spectrometry. The regioselective addition of the amine to the C-6 position of quinone 14 can be explained by the electron-releasing effect of the nitrogen atom, which is conjugated with the C-5 carbonyl and leaves the C₆=C₇=C₈=O fragment as the more electrophilic Michael acceptor moiety in the quinone.³³ This was confirmed by calculation of the Mulliken charges at both positions, which underscore the higher electrophilicity of C-6 (Scheme 1).

2.3. Biological evaluation

To evaluate the biological anti-AD MTDL profile of 2–6, we first assessed their inhibitory activity against human ChE enzymes, and then their antioxidant effects in neuronal cells. Following hepatotoxicity evaluation, we selected two nontoxic hybrids to be progressed to the anti-amyloid aggregation assay.

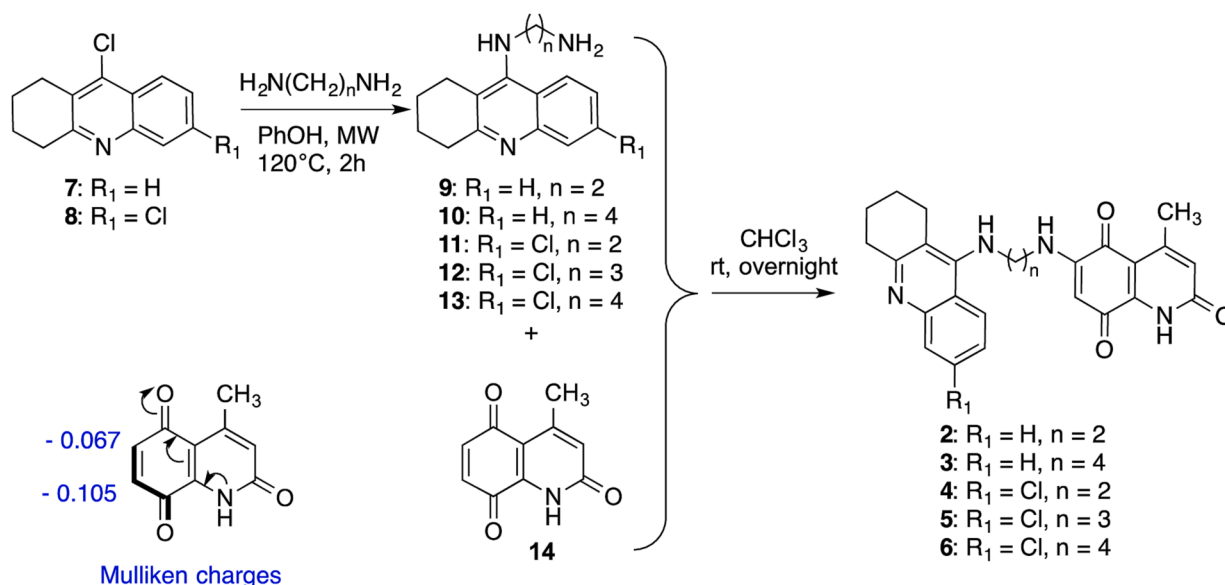
2.4. Inhibition of human AChE and BChE

To verify whether 2–6 shared the ChE inhibition properties of tacrine and the parent compound (1), we evaluated their inhibitory potency against human recombinant AChE (*hAChE*) and BChE from human serum (*hBChE*). All hybrids 2–6 turned out to be effective inhibitors of *hAChE*, with IC₅₀ values spanning nanomolar concentrations (Table 2). Notably, 3, 5 and 6 were significantly more active than tacrine, but less potent than 1. However, the presence of a given tacrine fragment seemed to have a significant effect on the inhibitory activity, as well as the number of methylene units of the linker. In agreement with the activity and selectivity profile of the starting fragments, i.e., tacrine and 6-chlorotacrine, hybrids carrying the 6-chlorotacrine moiety (4–6) displayed the highest potency for AChE and the best selectivity over BChE. Moreover, hybrid 2 and 4 featuring a linker of 2-methylene units exhibited lower inhibitory potency towards AChE (IC₅₀ values of 667 and 121 nM, respectively) compared to 3 and 6 (IC₅₀ values of 58.3 and 5.58 nM, respectively), which bear a 4-methylene based linker. Of note, 2 and 3 showed a balanced dual AChE/BChE inhibitory activity. Numerous studies demonstrated a shift of acetylcholine hydrolyzing activity, from AChE to BChE, along with the disease progression as a consequence of the progressive decline of the cholinergic system.³⁴ Accordingly, AChE levels gradually reduce, whereas BChE levels remain unaltered or increase.³⁵ Hence, AChE/BChE dual inhibitors might offer superior beneficial therapeutic effects for AD treatment than selective

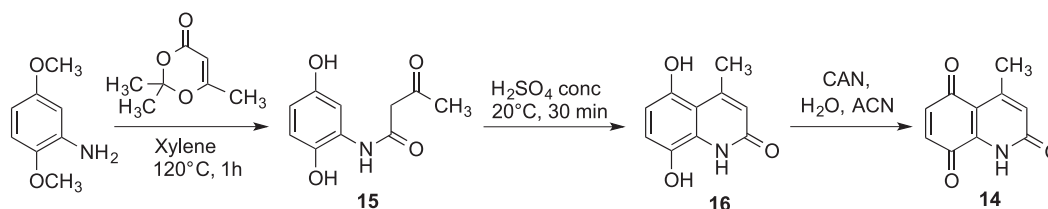
Table 1

In silico drug-likeness and BBB permeability profile of 2–6 compared with 1.

Entry	MW	logP	tPSA	Rotatable Bonds	HBD	HBA	Lipinski Violation	Oral Bioavailability	BBB permeability
1	447.91	5.64	92.57	5	3	6	1	Good	BBB+
2	428.48	2.95	105.20	5	3	7	0	Good	BBB+
3	456.54	3.66	105.20	7	3	7	0	Good	BBB+
4	462.93	3.58	105.20	5	3	7	0	Good	BBB+
5	476.95	3.93	105.20	6	3	7	0	Good	BBB+
6	490.98	4.29	105.20	7	3	7	0	Good	BBB+



Scheme 1. Synthesis of hybrids 2–6.



Scheme 2. Synthesis of 4-methylquinoline-2,5,8(1H)-trione 14.

Table 2
Cholinesterase inhibitory activities of 2–6 and reference compounds.

Compound	IC ₅₀ (nM)		SI ^a
	hAChE	hBChE	
2	667 ± 27	182 ± 8	0.27
3	58.3 ± 2.3	109 ± 36	1.87
4	121 ± 6	2100 ± 90	17.4
5	11.1 ± 0.4	1340 ± 80	121
6	5.58 ± 0.1	2830 ± 110	507
1 ^b	0.72 ± 0.06	542 ± 16	752
tacrine	415 ± 38	35 ± 7	0.08
6-chlorotacrine ^c	14.5 ± 0.9	505 ± 28	34.8

^a Selectivity Index (SI) is determined as the ratio $hBChE IC_{50}/hAChE IC_{50}$.

^b Data from ref.¹⁸;

^c Data from ref.³⁶.

AChEIs.

2.5. AChE docking studies

To provide insights into the binding modes of 2–6 and to better understand the experimental inhibitory data, we performed molecular docking calculations using the crystal structure of *Torpedo californica* AChE (TcAChE) in complex with 1 (PDB ID: 4TVK).¹⁸ To validate our protocol, we first carried out a redocking of 1 to the TcAChE binding site and the docking pose superimposed the crystallized ligand within a RMSD < 1.5 Å (data not shown). Overall, 2–6 showed a highly similar orientation to 1 and suitable conformational flexibility and length. The tacrine moiety spanned the catalytic site, while the quinolinetrione protruded toward the gorge entrance. Fig. 2 depicted the putative

binding modes of the less and most active AChE inhibitors 2 and 6, respectively. In contrast to the experimental inhibitory data, the results of the *in silico* studies showed no remarkable differences between the binding modes of 2 and 6, possibly suggesting the critical role of the 6-chlorotacrine fragment in AChE recognition. In both cases, the endocyclic nitrogen of the tetrahydroacridine ring interacted through a H-bond with the carbonyl oxygen of the catalytic residue His440, as reported and observed also for tacrine. Additionally, this fragment engaged π - π interactions with the aromatic rings of Trp84 and Phe330. On the other hand, the 4-methylquinoline-2,5,8(1H)-trione is embedded in a pocket lined with several aromatic residues (Tyr70, Tyr121, and Tyr334). Moreover, in the case of TcAChE-2 complex, the carbonyl oxygen of quinolinetrione formed a H-bond with the hydroxyl group of Tyr70 (Fig. 2A). Whereas 6, thanks to a linker of four methylene units, interacted by means of two H-bonds with the hydroxyl group of Tyr70 between the carbonyl oxygen and the lactam nitrogen (Fig. 2B). An additional aromatic interaction with Trp279 and the quinolinetrione of 6 further stabilized TcAChE-6 complex.

2.6. Antioxidant effects against menadione-induced oxidative stress of SH-SY5Y cells

Oxidative stress is a major player in neuronal degeneration and several studies have demonstrated that it is an early occurring condition in AD.³⁷ Several quinones have been reported as potential antioxidants against AD,^{24,38,39,40} however, it is well known that quinones may show a double-edged profile acting as prooxidant and/or antioxidant and ultimately may exert cytotoxic versus cytoprotective biological properties.²¹ Thus, to mimic oxidative damage, we treated neuroblastoma cells (SH-SY5Y) with menadione, a synthetic naphthoquinone known to

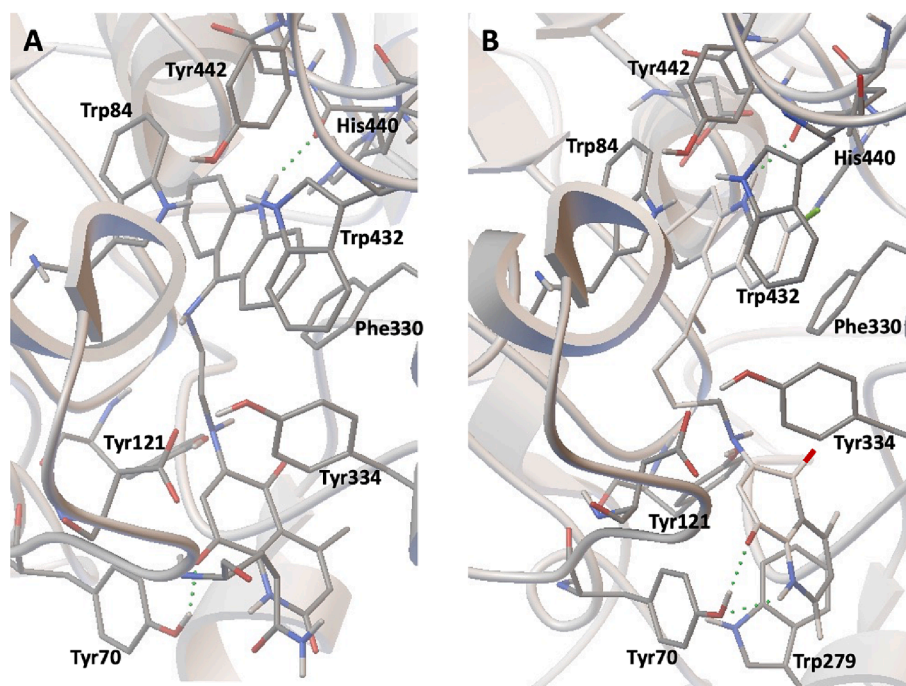


Fig. 2. Putative binding modes of **2** (A) and **6** (B) with TcAChE (PDB ID: 4TVK). The interacting residues are highlighted, and H-bonds are shown in green dotted lines.

induce oxidative stress, leading to mitochondrial damage and cell death.^{41,42} The effect of **2–6** in counteracting reactive oxygen species (ROS) production by menadione in SH-SY5Y cells was examined by using 2',7'-dichlorofluorescein diacetate as fluorescence probe, in comparison with tacrine and the antioxidant water-soluble analog of vitamin E, Trolox, as reference compound. As expected, treatment with 25 μ M menadione increased ROS production compared to control cells, which was totally reversed to the basal level with 10 μ M of Trolox (Fig. 3). By contrast, tacrine was not able to counteract menadione-induced ROS production. A similar trend was shown by 6-chlorotacrine hybrids **4** and **6**. Encouragingly, cells treated with unsubstituted tacrine derivative **3** showed a slight, significant decrease of ROS levels. However, **2** and **5** turned out to act as prooxidant molecules. Notwithstanding that we evaluated the antioxidant potential of **2–6** in a cell-based assay, their reactivities may be different and dependent on their subcellular localization, thus acting both as antioxidant and pro-oxidant molecules.

2.7. Cytotoxicity in human hepatoma cell line (HepG2)

Hepatotoxicity would be of importance for the overall drug-likeness of **2–6**, as tacrine was withdrawn from the market because of its hepatotoxicity and quinones are known for their cytotoxicity, especially for hepatocytes. Indeed, **1** was reported to decrease human hepatoma cell line (HepG2) viability by 25% at 10 μ M.¹⁸ Thus, experiments were performed in HepG2 cells, in comparison with tacrine and parent compound **1** (Fig. 4). After 24 h incubation at 1–100 μ M, a concentration-dependent decrease in cell viability was observed for all compounds. At 1 μ M, none of the hybrids showed significant cytotoxicity. Notably, **2** and **3**, carrying the unsubstituted tacrine moiety, demonstrated a good safety profile also at 10 μ M concentration, by slightly decreasing cell viability by 12% and 14% respectively. Conversely, **4–6** featuring a 6-chlorotacrine fragment, reduced cell viability by 50% at 10 μ M and were more toxic than **1**. At 100 μ M, all compounds were significantly toxic. Thus, we can postulate that both the quinone and tacrine substructures contribute to the overall hepatotoxicity profile of this class of hybrids.

2.8. Inhibition of A β_{1-42} self-aggregation

As stated above, the reevaluation of the amyloid hypothesis with the approval of two amyloid-removing antibodies, is likely making the amyloid cascade one of the most validated drug targets in AD drug discovery. Owing the limitation of the antibodies, we are interested in developing MTDLs able to interfere with A β aggregation. To verify the success of our design strategy, we ascertained if the quinolinetrione scaffold may exhibit a similar A β self-aggregation inhibition profile to that of the quinone moiety of **1** (Table 3). Thus, we evaluated the A β_{1-42} self-aggregation inhibition of the non-hepatotoxic hybrids **2–3** and compared their activity with those of **1** and starting tacrine. Gratifyingly, **2–3** displayed an inhibition of A β_{1-42} self-aggregation at 10 μ M similar to that of the parent compound **1** and similar to that exerted by the known inhibitor curcumin.⁴³ In agreement with previous reports,¹⁸ tacrine was inactive in our experimental setting. All this corroborates our starting idea that a 4-methylquinoline-2,5,8(1H)-trione moiety can effectively modulate the A β aggregation process by playing a role similar to that of juglone in **1**.

3. Conclusion

AD is the most common neurodegenerative disease. Cholinergic neurotransmission deficits, amyloid- β misfolding and aggregation, and excessive ROS production contribute to AD neurodegeneration. In this study, starting from a previously reported tacrine-quinone derivative **1**, we have developed a series of hybrids **2–6** by replacing the juglone moiety of **1** with that of quinolinetrione, a scaffold underexplored from a medicinal chemistry point of view and with no precedence in the AD (multi-target)-drug discovery field. Notably, hybrid **3**, featuring an unsubstituted tacrine fragment connected via a linker of four methylenes, not only preserved the ability of **1** to modulate multiple targets underlying AD, but also showed a slightly improved hepatotoxicity profile. It turned out to be a potent dual inhibitor of the cholinesterase enzymes with IC₅₀ values of 58.3 and 109 nM against hAChE and hBChE, respectively. Moreover, **3** displayed antioxidant properties in menadione-induced oxidative stress of SH-SY5Y cells. Importantly, at

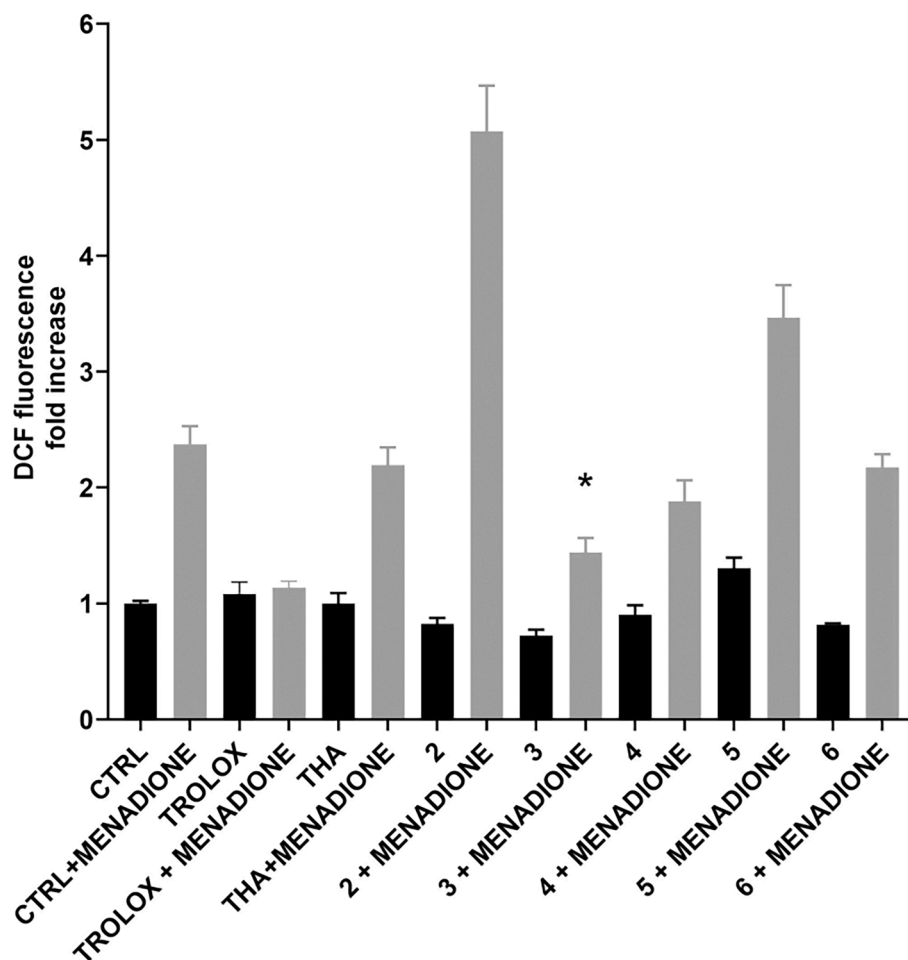


Fig. 3. Antioxidant effects against menadione-induced oxidative stress of SH-SY5Y cells. Reactive oxygen species were detected using the fluorescent probe DCFDA in cells treated with 10 μM of compounds 2–6, trolox, tacrine (THA) or vehicle (CTRL). Oxidative stress was induced with 25 μM of menadione. Each bar represents means \pm SEM of three independent experiments. Data were analyzed with an ordinary one-way ANOVA. * $p < 0.05$ compared to CTRL + menadione.

10 μM , it also showed a slightly lower cytotoxicity in HepG2 cells than 1 along with similarly good amyloid anti-aggregation properties. It should be noted that although both 1 and 3 showed greater hepatotoxicity than tacrine, they are endowed of amyloid anti-aggregation and antioxidant properties, which are not related to the tacrine scaffold.

Overall, this small set of MTDLs might help to better understand the complex interconnection between the different neurodegenerative pathways (cholinergic deficit, A β misfolding, and oxidative stress) and to design novel and more effective anti-AD hybrids based on a quinone substructure. Remarkably, we uncovered the potential of the 2,5,8(1H)-quinolinetrione scaffold, as a novel anti-amyloid aggregation and antioxidant motif, which may be exploited in future anti-AD multi-target drug discovery endeavors.

Above all, this initial set of tacrine-2,5,8(1H)-quinolinetrione MTDLs demonstrated their anti-AD potential, and further SAR optimization focused on the exploration of different substituents on the tacrine ring and the functionalization of the lactam nitrogen of 2,5,8(1H)-quinolinetrione is underway for subsequent hit-to-lead optimization studies.

4. Experimental section

4.1. Chemistry

All reagents and solvents were supplied from Merck, Madrid, Spain, and Scharlau, Barcelona, Spain and used without further purification with exception of 2,5-dimethoxyaniline, which was filtered through a pad of silica gel, eluting with diethyl ether, before use. Reactions were

monitored by thin layer chromatography (TLC) on aluminum plates coated with silica gel and fluorescent indicator (layer: 0.20 mm silica gel 60 with a fluorescent indicator UV254, from Merck, Madrid, Spain). Microwave-assisted reactions were performed on a CEM Discover focused microwave reactor, operating with an irradiation power of 150 W. Chromatographic separations were performed using silica gel SDS 60 ACC. NMR spectroscopic data were recorded using a Bruker Avance 250 spectrometer (Bruker, Rivas-Vaciamadrid, Spain) operating at 250 MHz for ^1H NMR and 63 MHz for ^{13}C NMR (CAI de Resonancia Magnética Nuclear, Madrid, Spain), using the residual non-deuterated solvent as an internal standard. Chemical shifts (δ) are given in ppm and the multiplicities of ^1H signals indicated as: s (singlet), d (doublet), t (triplet), q (quartet), m (multiplet), bs (broad singlet). Coupling constants (J) are given in Hertz (Hz). Melting points (Mp) were determined with a Stuart Scientific apparatus, SMP3 Model. MS spectra were produced with an electrospray-ionization mass spectrometer (ESI-MS) by the Unidad de Espectrometría de Masas (Universidad Complutense de Madrid). Elemental analyses were determined by the microanalysis facility of Universidad Complutense (Unidad de Microanálisis Elemental), using a Leco 932 combustion microanalyzer. Elemental analysis confirmed that all final compounds are $> 95\%$ purity. Analyses were within $\pm 0.4\%$ of the theoretical values.

4.2. General procedure for the synthesis of quinoline-2,5,8(1H)trione-tacrine hybrids (2–6)

The suitable intermediate (9–13, 1 eq.) was dissolved in 1 mL of

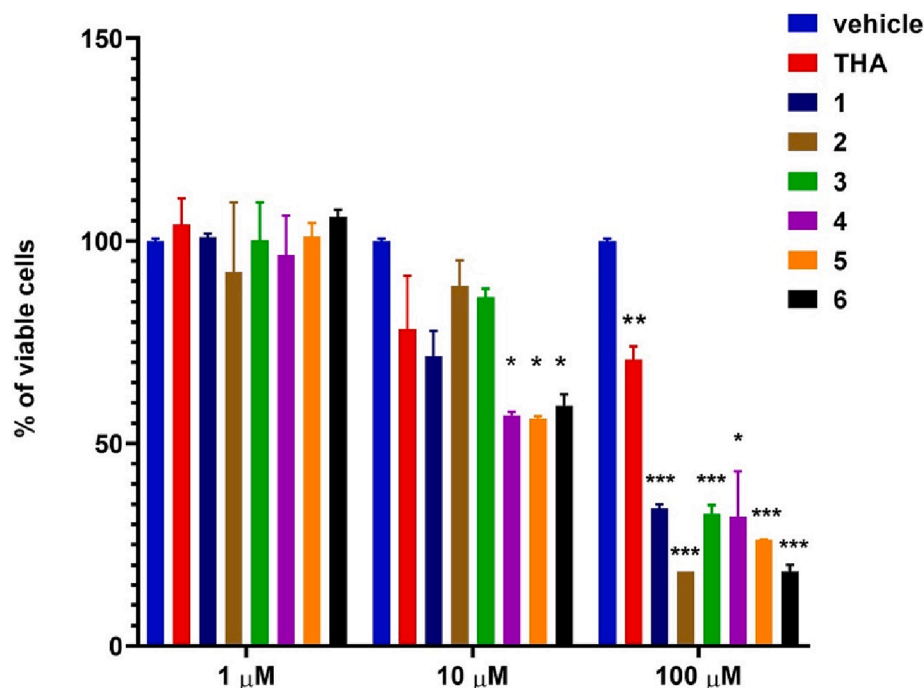


Fig. 4. Cell viability in HepG2 cells. Cell viability was determined by MTT assay in HepG2 cells. Cells were treated with increasing concentrations of compounds 3–8 in comparison with tacrine (THA) and vehicle (1, 10, 100 μM) for 24 h and cell viability was assessed by MTT assay. Each bar represents means ± SEM of two independent experiments. Data were analyzed with an ordinary one-way ANOVA. * $p < 0.05$ compared to vehicle.

Table 3

Inhibition of A β_{1-42} self-aggregation of hybrids 2–3 and reference compounds.

Compound	Inhibition of A β_{1-42} self-aggregation (%) ± SEM [I] = 10 μM
2	34.6 ± 3.7
3	33.4 ± 4.2
1 ^a	37.5 ± 4.9
tacrine	<5%
curcumin	34.5 ± 1.4

^a Data taken from ref. ¹⁸.

CHCl₃ and was added dropwise to the solution of quinoline-2,5,8(1H)trione **14** (1.2–1.4 eq.) in CHCl₃. The reaction mixture was stirred for 24 h at room temperature in an open round-bottom flask. The crude residue was purified by flash chromatography using CH₂Cl₂/EtOH/NEt₃ (9.4:0.6:0.05) as eluent. The residue was then recrystallized from hexane/CHCl₃ to give the final compound (2–6) as purple/red solid.

4-Methyl-6-((2-((1,2,3,4-tetrahydroacridin-9-yl)amino)ethyl)amino)quinoline-2,5,8(1H)-trione (2). Prepared from N¹-(1,2,3,4-tetrahydroacridin-9-yl)ethane-1,2-diamine **9** (99.6 mg, 0.41 mmol) and 4-methylquinoline-2,5,8(1H)-trione **14** (109.3 mg, 0.58 mmol). Yield: 23%. Mp: 198 °C (decomposed). ¹H NMR (250 MHz, MeOD/CDCl₃) δ 8.17 (d, $J = 8.5$ Hz, 1H), 7.70 (s, 2H), 7.50–7.42 (m, 1H), 6.44 (s, 1H), 5.58 (s, 1H), 4.12–4.01 (m, 2H), 3.67–3.55 (m, 2H), 3.04–2.90 (m, 2H), 2.67 (d, $J = 14.7$ Hz, 2H), 2.53 (s, 3H), 2.02–1.80 (m, 4H). ¹³C NMR (63 MHz, MeOD/CDCl₃) δ 178.3, 175.0, 161.3, 159.0, 152.1, 149.4, 146.0, 142.0, 135.2, 129.2, 127.3, 124.7, 123.7, 122.2, 120.1, 117.5, 111.6, 95.6, 45.9, 43.49, 32.8, 25.1, 22.7, 22.3, 22.2. HRMS (ESI): Calcd for C₂₅H₂₅N₄O₃ ([M + H]) m/z : 429.1932; found: ESI m/z : 429.1917.

4-Methyl-6-((4-((1,2,3,4-tetrahydroacridin-9-yl)amino)butyl)amino)quinoline-2,5,8(1H)-trione (3). Prepared from N¹-(1,2,3,4-tetrahydroacridin-9-yl)butane-1,4-diamine **10** (120 mg, 0.44 mmol) and 4-methylquinoline-2,5,8(1H)-trione **14** (103.2 mg, 0.53 mmol). Yield: 34%. Mp: 150 °C (decomposed). ¹H NMR (250 MHz, MeOD/CDCl₃) δ 7.92 (d, $J = 7.8$ Hz, 1H), 7.81 (d, $J = 8.3$ Hz, 1H), 7.51 (t, $J = 7.0$ Hz, 1H), 7.31 (d, $J = 7.4$ Hz, 1H), 6.36 (d, $J = 1.1$ Hz, 1H), 5.47 (s, 1H), 3.60

(br s, 2H), 3.61–3.48 (m, 2H), 3.25–3.14 (m, 2H), 3.02–2.87 (m, 2H), 2.68–2.54 (m, 2H), 2.46 (d, $J = 1.0$ Hz, 3H), 1.91–1.78 (m, 4H), 1.78–1.64 (m, 4H). ¹³C NMR (63 MHz, MeOD/CDCl₃) δ 178.5, 174.7, 161.3, 156.6, 152.0, 151.9, 149.3, 144.8, 142.3, 129.6, 125.9, 124.3, 123.5, 123.0, 119.0, 115.2, 111.6, 95.1, 49.0, 42.4, 32.1, 28.7, 25.3, 24.7, 22.6, 22.1, 22.1. HRMS (ESI): Calcd for C₂₇H₂₉N₄O₃ ([M + H]) m/z : 457.2240; found: 457.2248.

6-((2-((6-Chloro-1,2,3,4-tetrahydroacridin-9-yl)amino)ethyl)amino)-4-methylquinoline-2,5,8(1H)-trione (4). Prepared from N¹-(6-chloro-1,2,3,4-tetrahydroacridin-9-yl)ethane-1,2-diamine **11** (106.0 mg, 0.38 mmol) and 4-methylquinoline-2,5,8(1H)-trione **14** (126.8 mg, 0.67 mmol). Yield: 45%. Mp: 204 °C (decomposed). ¹H NMR (250 MHz, MeOD/CDCl₃) δ 7.79 (m, 2H), 7.24 (d, $J = 2.0$ Hz, 1H), 6.41 (s, 1H), 5.51 (s, 1H), 3.71 (t, $J = 5.8$ Hz, 2H), 3.42 (m, 2H), 3.40 (br s, 2H), 3.00–2.87 (m, 2H), 2.70–2.57 (m, 2H), 2.48 (s, 3H), 1.92–1.77 (m, 4H). ¹³C NMR (75 MHz, MeOD/CDCl₃) δ 178.1, 174.8, 161.1, 159.6, 151.8, 150.1, 149.1, 146.8, 141.8, 134.6, 126.4, 125.1, 123.7, 123.6, 118.6, 117.5, 111.4, 95.5, 49.0, 45.8, 43.3, 33.0, 24.8, 22.5, 22.1. HRMS (ESI): Calcd for C₂₅H₂₄ClN₄O₃ ([M + H]) m/z : For the ³⁵Cl isotope, 463.1537; found: 463.1558. For the ³⁷Cl isotope, 465.1507; found: 465.1522.

6-((3-((6-Chloro-1,2,3,4-tetrahydroacridin-9-yl)amino)propyl)amino)-4-methylquinoline-2,5,8(1H)-trione (5). Prepared from N¹-(6-chloro-1,2,3,4-tetrahydroacridin-9-yl)propane-1,3-diamine **12** (107.0 mg, 0.37 mmol) and 4-methylquinoline-2,5,8(1H)-trione **14** (84.0 mg, 0.44 mmol). Yield: 39%. Mp: 207 °C (decomposed). ¹H NMR (250 MHz, CDCl₃) δ 7.85 (d, $J = 2.0$ Hz, 1H), 7.83 (d, $J = 4.7$ Hz, 1H), 7.30–7.14 (m, 1H), 6.60 (t, $J = 5.7$ Hz, 1H), 6.41 (d, $J = 1.0$ Hz, 1H), 5.51 (s, 1H), 3.52 (t, $J = 5.8$ Hz, 2H), 3.30–3.18 (m, 2H), 3.06–2.94 (m, 2H), 2.72–2.61 (m, 2H), 2.51 (s, 3H), 1.95–1.84 (m, 4H), 1.83–1.65 (m, 4H). ¹³C NMR (63 MHz, CDCl₃) δ 178.6, 174.8, 160.8, 160.1, 151.6, 150.1, 149.1, 148.0, 142.2, 134.3, 127.8, 125.0, 124.0, 123.9, 118.8, 117.4, 111.3, 95.5, 46.6, 40.7, 34.0, 29.9, 25.0, 22.9, 22.7, 22.3. HRMS (ESI): Calcd for C₂₆H₂₆ClN₄O₃ ([M + H]) m/z : For the ³⁵Cl isotope, 477.1693; found: 477.1711. For the ³⁷Cl isotope, 479.1664; found: 479.1682.

6-((4-((6-Chloro-1,2,3,4-tetrahydroacridin-9-yl)amino)butyl)amino)-

4-methylquinoline-2,5,8(1H)-trione (6). Prepared from N¹-(6-chloro-1,2,3,4-tetrahydroacridin-9-yl)butane-1,4-diamine 13 (114.0 mg, 0.38 mmol) and 4-methylquinoline-2,5,8(1H)-trione 14 (85.5 mg, 0.45 mmol). Yield: 38%. Mp: 175 °C (decomposed). ¹H NMR (250 MHz, CDCl₃) δ 7.85 (d, *J* = 2.0 Hz, 1H), 7.83 (d, *J* = 4.7 Hz, 1H), 7.30–7.14 (m, 1H), 6.60 (t, *J* = 5.7 Hz, 1H), 6.41 (d, *J* = 1.0 Hz, 1H), 5.51 (s, 1H), 3.52 (t, *J* = 5.8 Hz, 2H), 3.30–3.18 (m, 2H), 3.06–2.94 (m, 2H), 2.72–2.61 (m, 2H), 2.51 (s, 3H), 1.95–1.84 (m, 4H), 1.83–1.65 (m, 4H). ¹³C NMR (63 MHz, CDCl₃) δ 178.6, 174.8, 160.7, 159.5, 151.6, 150.6, 149.2, 147.6, 142.2, 134.4, 127.3, 124.7, 124.4, 123.9, 118.4, 116.4, 111.3, 95.4, 48.8, 42.7, 33.8, 29.1, 25.5, 24.8, 22.9, 22.6, 22.3. HRMS (ESI): Calcd for C₂₇H₂₈ClN₄O₃ ([M + H]⁺) *m/z*: For the ³⁵Cl isotope, 491.1850; found: 491.1868. For the ³⁷Cl isotope, 493.1820; found: 493.1839.

4.3. Molecular docking

The crystal structures of *Torpedo californica* TcAChE in complex with 1 was retrieved from Protein Data Bank (PDB ID: 4TVK).¹⁸ AutoDock4⁴⁴ was used to carry out molecular docking of 2–6 to TcAChE. The cleaned AChE structure and the compound structures were imported into AutoDockTools (ADT) to generate the coordinates (pdbqt files) of the receptor and ligand for docking studies. The grid box was centered on the binding pocket of the receptor, and it was resized by increasing the number of grid points in xyz (50 × 50 × 50 Å) to generate a gpf file (grid parameter file). The affinity map files were generated by using autogrid4 with the gpf file. Then, AutoDock's Lamarckian genetic algorithm was run with default options except in the number of runs (50) and the population size (50) to perform docking of compounds. The compounds were ranked based on the binding energy, clustered and only one unique binding pose was selected by visually inspection.

4.4. Inhibition of human AChE and BChE

The inhibitory activity of the target compounds toward recombinant human AChE (Sigma-Aldrich, Milan, Italy) and human serum BChE (Sigma-Aldrich, Milan, Italy) was assessed by Ellman's method,⁴⁵ using tacrine and 6-chlorotacrine as reference compounds. Stock solutions of compounds to be tested were made in MeOH (2 mM). Stock solution of hAChE was prepared in 0.1 M potassium phosphate (pH 8.0) containing 0.1% Triton X-100, whereas the stock solution of hBChE was prepared in 0.1% aqueous gelatin. The assay solution consisted of 0.02 unit mL⁻¹ of the enzyme, 340 μM 5,5'-dithiobis(2-nitrobenzoic acid), and 550 μM of substrate (acetylthiocholine iodide or butyrylthiocholine iodide for AChE and BChE, respectively) in 0.1 M potassium phosphate (pH 8.0). Blank solutions containing all components except the enzymes were prepared to account for the non-enzymatic hydrolysis of substrate. Prior the addition of the substrate, assay solutions were incubated at 37 °C for 20 min. After incubation, reaction was started by the addition of substrate and the increase of absorbance at 412 nm was monitored for 240 s using a Jasco V-530 double beam spectrophotometer equipped with thermostated cuvette holders (37 °C). For each tested compound, five increasing concentrations were assayed in order to achieve inhibition percentages of 20–80%. Each concentration was assayed in triplicate. IC₅₀ values were calculated from the inhibition plot (% inhibition vs log [inhibitor]) and are expressed as mean ± SEM. Each IC₅₀ value is the average of at least two experiments, each performed in triplicate.

4.5. Cell viability in HepG2 cells

Human liver cancer HepG₂ cell line was cultured in Dulbecco Modified Eagle's medium (DMEM) containing 4.5 g/L glucose, 2 mM glutamine, 1% penicillin/streptomycin, and 10% FBS (Fetal Bovine Serum). Cells were grown at 37 °C in 5% CO₂ with saturating humidity. Cell viability was assessed by MTT assay. HepG₂ cells were seeded in 96-well plates at 2 × 10³ cells/well in complete DMEM. After 24 h of incubation at 37 °C in 5% CO₂ to allow adhesion, cells were washed with

HBSS and incubated with different concentrations of compounds or vehicle in complete DMEM for 24 h. After this time, cells were washed with HBSS buffer (156 mM NaCl, 3 mM KCl, 2 mM MgSO₄, 1.25 mM KH₂PO₄, 2 mM CaCl₂, 10 mM glucose, and 10 mM HEPES; pH adjusted to 7.4 with NaOH) and incubated with 300 μM of MTT (3-(4,5-dimethylthiazol-2-yl)-2,5-diphenyltetrazolium bromide) dissolved in DMEM. After 1 h, the medium was removed and formazan salts were solubilized in 150 μL of dimethyl sulfoxide (DMSO) for 15 min placing the multi-well in an orbital shaker for 15 min in the dark. The absorbance of each well was measured at 575 nm using a plate reader (Enspire, Perkin Elmer, Waltham, MA, USA).

4.6. Antioxidant activity in SH-SY5Y cells

Antioxidant activity was assayed in SH-SY5Y cells using the reactive oxygen species indicator 2',7'-dichlorodihydrofluorescein diacetate (DCFDA, Thermo Fisher Scientific, Waltham, MA, USA). Cells were seeded in 96-well plates at 2 × 10⁴ cells/well (Oптиplate, Perkin Elmer). After 24 h to allow adhesion, the cells were incubated with 10 μM of different compounds for 24 h at 37 °C in 5% CO₂. After this time, cells were washed with Hank's balanced salt solution (HBSS) and treated with 25 μM of menadione or vehicle dissolved in complete DMEM for 4 h. After this time, cells were washed with HBSS and incubated with DCFDA (2',7'-dichlorofluorescein diacetate, DCFH-DA, Thermo Fisher) dissolved in DMEM for 30 min. Finally, the cells were washed again with HBSS and the fluorescence value in each well was measured (λ_{exc} = 485 nm; λ_{em} = 535 nm) with a plate reader (Enspire, Perkin Elmer). Fluorescence emission was normalized on protein content measured by the Lowry method. Experiments were performed in triplicate. *p.

4.7. Inhibitory potency on Aβ₁₋₄₂ Self-Aggregation

1,1,1,3,3,3-Hexafluoro-2-propanol (HFIP)-pretreated Aβ₁₋₄₂ samples (Bachem AG, Switzerland) were solubilized with a CH₃CN/0.3 mM Na₂CO₃/250 mM NaOH (48.4/48.4/3.2) mixture to obtain a 500 μM stock solution.^{46,47} 2.0 mM stock solutions of the inhibitors were prepared in methanol and diluted in the assay buffer up to the required screening concentration. The determination of antiaggregating activity was performed by incubating for 24 h Aβ₁₋₄₂ pretreated samples in 10 mM phosphate buffer (pH = 8.0) containing 10 mM NaCl, at 30 °C (Thermomixer, Eppendorf, Italy) (final Aβ concentration = 50 μM) with and without tested inhibitors at 10.0 μM (Aβ/inhib. = 5/1). Blanks containing tested inhibitors were also tested. To quantify Aβ fibril formation, after incubation, each sample was diluted to 2.0 mL with a 50 mM glycine – NaOH buffer (pH 8.5) containing 1.5 μM thioflavin T.⁴⁶ A 300-s time scan of fluorescence intensity was carried out (λ_{exc} = 446 nm; λ_{em} = 490 nm), and values at plateau were averaged after subtracting the background fluorescence of 1.5 μM thioflavin T solution. The fluorescence intensities were compared, and the percent inhibition due to the presence of the tested inhibitor was calculated.

Declaration of Competing Interest

The authors declare that they have no known competing financial interests or personal relationships that could have appeared to influence the work reported in this paper.

Data availability

Data will be made available on request.

Acknowledgments

This work was supported by the University of Bologna (Grants RFO) and Ministerio de Ciencia e Innovación, Spain (grant PID2021-124983OB-I00).

Appendix A. Supplementary data

Supplementary data to this article can be found online at <https://doi.org/10.1016/j.bmc.2023.117419>.

References

- Knopman DS, Amieva H, Petersen RC, et al. Alzheimer Disease. *Nat Rev Dis Primers*. 2021;7:33. <https://doi.org/10.1038/s41572-021-00269-y>.
- International, A. D. Dementia Statistics. <https://www.alzint.org/about/dementia-facts-figures/dementia-statistics/>.
- Wang H, Zhang H. Reconsideration of Anticholinesterase Therapeutic Strategies against Alzheimer's Disease. *ACS Chem Neurosci*. 2019;10:852–862. <https://doi.org/10.1021/acscchemneuro.8b00391>.
- García-Ayllón MS, Small DH, Avila J, Sáez-Valero J. Revisiting the Role of Acetylcholinesterase in Alzheimer's Disease: Cross-Talk with P-Tau and β -Amyloid. *Front Mol Neurosci*. 2011;4:22. <https://doi.org/10.3389/fnmol.2011.00022>.
- Hardy JA, Higgins GA. Alzheimer's disease: the amyloid cascade hypothesis. *Science*. 1992;256:184–185. <https://doi.org/10.1126/science.1566067>.
- Karran E, De Strooper B. The amyloid hypothesis in Alzheimer disease: new insights from new therapeutics. *Nat Rev Drug Discov*. 2022;21:306–318. <https://doi.org/10.1038/s41573-022-00391-w>.
- Reardon S. FDA Approves Alzheimer's Drug Lecanemab amid Safety Concerns. *Nature*. 2023;613:227–228. <https://doi.org/10.1038/d41586-023-00030-3>.
- Small Molecules Reenter the Ring in the Quest to Treat Alzheimer's Disease. C&EN Global Enterprise, 2023, 101, 20–25. <https://doi.org/10.1021/cen-10109-cover>.
- Butterfield DA, Boyd-Kimball D. Oxidative Stress, Amyloid- β Peptide, and Altered Key Molecular Pathways in the Pathogenesis and Progression of Alzheimer's Disease. *J Alzheimers Dis*. 2018;62:1345–1367. <https://doi.org/10.3233/JAD-170543>.
- Butterfield DA, Halliwell B. Oxidative Stress, Dysfunctional Glucose Metabolism and Alzheimer Disease. *Nat Rev Neurosci*. 2019;20:148–160. <https://doi.org/10.1038/s41583-019-0132-6>.
- Viegas C, Fraga CAM, Sousa ME, Tarozzi A. Editorial: oxidative stress: how has it been considered in the design of new drug candidates for neurodegenerative diseases? *Front Pharmacol*. 2020;11, 609274. <https://doi.org/10.3389/fphar.2020.609274>.
- Di Domenico F, Pupo G, Giraldo E, et al. Oxidative Signature of Cerebrospinal Fluid from Mild Cognitive Impairment and Alzheimer Disease Patients. *Free Radic Biol Med*. 2016;91:1–9. <https://doi.org/10.1016/j.freeradbiomed.2015.12.004>.
- Cummings J, Lee G, Nahed P, et al. Alzheimer's Disease Drug Development Pipeline: 2022. *Alzheimers Dement (N Y)*. 2022;8:e12295.
- Persson T, Popescu BO, Cedazo-Minguez A. Oxidative Stress in Alzheimer's Disease: Why Did Antioxidant Therapy Fail? *Oxid Med Cell Longev*. 2014;2014, 427318. <https://doi.org/10.1155/2014/427318>.
- Albertini, C.; Salerno, A.; de Sena Murteira Pinheiro, P.; Bolognesi, M. L. From Combinations to Multitarget-Directed Ligands: A Continuum in Alzheimer's Disease Polypharmacology. *Med Res Rev*, 2020. <https://doi.org/10.1002/med.21699>.
- Abbott A. Conquering Alzheimer's: A Look at the Therapies of the Future. *Nature*. 2023;616:26–28. <https://doi.org/10.1038/d41586-023-00954-w>.
- Cavalli A, Bolognesi ML, Minarini A, et al. Multi-Target-Directed Ligands to Combat Neurodegenerative Diseases. *J Med Chem*. 2008;51:347–372. <https://doi.org/10.1021/jm7009364>.
- Nepovimova E, Uliassi E, Korabecny J, et al. Multitarget Drug Design Strategy: Quinone-Tacrine Hybrids Designed to Block Amyloid- β Aggregation and to Exert Anticholinesterase and Antioxidant Effects. *J Med Chem*. 2014;57:8576–8589. <https://doi.org/10.1021/jm5010804>.
- Romero A, Cacabelos R, Oset-Gasque MJ, Samadi A, Marco-Contelles J. Novel Tacrine-Related Drugs as Potential Candidates for the Treatment of Alzheimer's Disease. *Bioorg Med Chem Lett*. 2013;23:1916–1922. <https://doi.org/10.1016/j.bmcl.2013.02.017>.
- Bautista-Aguilera Ó, Ismaili L, Iriepa I, et al. Tacrines as Therapeutic Agents for Alzheimer's Disease. V. Recent Developments. *Chem Rec*. 2021;21:162–174. <https://doi.org/10.1002/ctr.202000107>.
- Bolton JL, Dunlap T. Formation and biological targets of quinones: cytotoxic versus cytoprotective effects. *Chem Res Toxicol*. 2017;30:13–37. <https://doi.org/10.1021/acs.chemrestox.6b00256>.
- Klopčić I, Dolenc MS. Chemicals and drugs forming reactive quinone and quinone imine metabolites. *Chem Res Toxicol*. 2019;32:1–34. <https://doi.org/10.1021/acs.chemrestox.8b00213>.
- Campora M, Francesconi V, Schenone S, Tasso B, Tonelli M. Journey on Naphthoquinone and Anthraquinone Derivatives: New Insights in Alzheimer's Disease. *Pharmaceuticals (Basel)*. 2021;14. <https://doi.org/10.3390/ph14010033>.
- Cavalli A, Bolognesi ML, Capsoni S, et al. A small molecule targeting the multifactorial nature of Alzheimer's disease. *Angew Chem Int Ed Engl*. 2007;46:3689–3692. <https://doi.org/10.1002/anie.200700256>.
- Chalupova K, Korabecny J, Bartolini M, et al. Novel Tacrine-Tryptophan hybrids: multi-target directed ligands as potential treatment for Alzheimer's disease. *Eur J Med Chem*. 2019;168:491–514. <https://doi.org/10.1016/j.ejmech.2019.02.021>.
- Gesto C, de la Cuesta E, Avendaño C, Emling F. Synthesis and Biological Activity of New 1,8-Diaza-2,9,10-Anthracenetrione Derivatives. *J Pharm Sci*. 1992;81:815–816. <https://doi.org/10.1002/jps.2600810819>.
- Banerjee P, Eckert AO, Schrey AK, Preissner R. ProTox-II: A Webserver for the Prediction of Toxicity of Chemicals. *Nucleic Acids Res*. 2018;46:W257–W263. <https://doi.org/10.1093/nar/gky318>.
- Lagorce D, Bousslama L, Becot J, Miteva MA, Villoutreix BO. FAF-Drugs4: Free ADME-Tox Filtering Computations for Chemical Biology and Early Stages Drug Discovery. *Bioinformatics*. 2017;33:3658–3660. <https://doi.org/10.1093/bioinformatics/btx491>.
- Liu H, Wang L, Lv M, et al. AlzPlatform: An Alzheimer's Disease Domain-Specific Chemogenomics Knowledgebase for Polypharmacology and Target Identification Research. *J Chem Inf Model*. 2014;54:1050–1060. <https://doi.org/10.1021/ci500004h>.
- Hu MK, Wu LJ, Hsiao G, Yen MH. Homodimeric Tacrine Congeners as Acetylcholinesterase Inhibitors. *J Med Chem*. 2002;45:2277–2282. <https://doi.org/10.1021/jm010308g>.
- Staderini M, Cabezas N, Bolognesi ML, Menéndez JC. Solvent- and Chromatography-Free Amination of π -Deficient Nitrogen Heterocycles under Microwave Irradiation. A Fast, Efficient and Green Route to 9-Aminoacridines, 4-Aminoquinolines and 4-Aminoquinazolines and Its Application to the Synthesis of the Drugs Amsacrine and Bistacrine. *Tetrahedron*. 2013;69:1024–1030. <https://doi.org/10.1016/j.tet.2012.11.083>.
- Avendaño C, de la Cuesta E, Gesto C. A Comparative Study of Synthetic Approaches to 1-Methyl-2,5,8(1H)-Quinolinetriene and 4-Methyl-2,5,8(1H)-Quinolinetriene. *Synthesis*. 1991;1991:727–730. <https://doi.org/10.1055/s-1991-26557>.
- Pérez J, Avendaño C, Menéndez JC. 1-Acylamino-1-Azadienes as an Alternative to 1-Dimethylamino-1-Azadienes in the Preparation of 1,8-Diazaanthracene-2,9,10-Triones. *Tetrahedron*. 1995;51(23):6573–6586. [https://doi.org/10.1016/0040-4020\(95\)00295-J](https://doi.org/10.1016/0040-4020(95)00295-J).
- Mushtaq G, Greig NH, Khan JA, Kamal MA. Status of Acetylcholinesterase and Butyrylcholinesterase in Alzheimer's Disease and Type 2 Diabetes Mellitus. *CNS Neurol Disord Drug Targets*. 2014;13:1432–1439. <https://doi.org/10.2174/1871527133666141023141545>.
- Giacobini E. Cholinesterases: New Roles in Brain Function and in Alzheimer's Disease. *Neurochem Res*. 2003;28:515–522. <https://doi.org/10.1023/a:1022869222652>.
- Rossi M, Freschi M, de Camargo Nascente L et al. Sustainable drug discovery of multi-target-directed ligands for Alzheimer's disease. *J Med Chem*, 2021, 64, 4972–4990. <https://doi.org/10.1021/acs.jmedchem.1c00048>.
- Nantachai G, Vasupanrajit A, Tunvirachaisakul C, Solmi M, Maes M. Oxidative stress and antioxidant defenses in mild cognitive impairment: a systematic review and meta-analysis. *Ageing Res Rev*. 2022;79, 101639. <https://doi.org/10.1016/j.arr.2022.101639>.
- Tao L, Xie J, Wang Y, et al. Protective Effects of Aloe-Emodin on Scopolamine-Induced Memory Impairment in Mice and H₂O₂-Induced Cytotoxicity in PC12 Cells. *Biol Med Chem Lett*. 2014;24:5385–5389. <https://doi.org/10.1016/j.bmcl.2014.10.049>.
- Mezeiova E, Janockova J, Andrys R, et al. 2-Propargylamino-Naphthoquinone Derivatives as Multipotent Agents for the Treatment of Alzheimer's Disease. *Eur J Med Chem*. 2021;211, 113112. <https://doi.org/10.1016/j.ejmech.2020.113112>.
- Perone R, Albertini C, Uliassi E, et al. Turning Donepezil into a Multi-Target-Directed Ligand through a Merging Strategy. *ChemMedChem*. 2021;16:187–198. <https://doi.org/10.1002/cmdc.202000484>.
- Loor G, Kondapalli J, Schriewer JM, Chandel NS, Vanden Hoek TL, Schumacker PT. Menadione Triggers Cell Death through ROS-Dependent Mechanisms Involving PARP Activation without Requiring Apoptosis. *Free Radic Biol Med*. 2010;49:1925–1936. <https://doi.org/10.1016/j.freeradbiomed.2010.09.021>.
- Kesari KK, Dhasmana A, Shandilya S, et al. Natural Biomolecule Picein Attenuates Menadione Induced Oxidative Stress on Neuroblastoma Cell Mitochondria. *Antioxidants (Basel)*. 2020;9. <https://doi.org/10.3390/antiox9060552>.
- Pagano K, Tomaselli S, Molinari H, Ragona L. Natural Compounds as Inhibitors of A β Peptide Aggregation: Chemical Requirements and Molecular Mechanisms. *Front Neurosci*. 2020;14, 619667. <https://doi.org/10.3389/fnins.2020.619667>.
- Morris GM, Huey R, Lindstrom W, et al. AutoDock4 and AutoDockTools4: Automated Docking with Selective Receptor Flexibility. *J Comput Chem*. 2009;30(16):2785–2791. <https://doi.org/10.1002/jcc.21256>.
- Ellman GL, Courtney KD, Andres V, Feather-Stone RM. A new and rapid colorimetric determination of acetylcholinesterase activity. *Biochem Pharmacol*. 1961;7:88–95. [https://doi.org/10.1016/0006-2952\(61\)90145-9](https://doi.org/10.1016/0006-2952(61)90145-9).
- Naiki H, Higuchi K, Nakakuki K, Takeda T. Kinetic analysis of amyloid fibril polymerization in vitro. *Lab Invest*. 1991;65:104–110.
- Bartolini M, Naldi M, Fiori J, et al. Kinetic Characterization of Amyloid-Beta 1–42 Aggregation with a Multimethodological Approach. *Anal Biochem*. 2011;414:215–225. <https://doi.org/10.1016/j.ab.2011.03.020>.